Structural and Morphology Changes in PrMnO₃ Manganite Induced by Ba (*x*=0.33) Doping

Nor Asmira Amaran[1], Norazila Ibrahim[1], Zakiah Mohamed[1,*]

[1] Faculty of Applied Sciences, Universiti Teknologi MARA, 40450 Shah Alam, Selangor, Malaysia

ARTICLE INFO	ABSTRACT
     	In this paper, we discuss the structural and morphology properties of the solid-state prepared $Pr_{0.67}Ba_{0.33}MnO_3$ perovskite manganite X-ray diffraction (XRD), scanning electron microscopy (SEM) and energy dispersive X-ray (EDX) analyses were utilised to examine the structure, morphology, and chemical composition. The compound exhibits a single phase with an orthorhombic perovskite structure with a *Pnma* space group without any impurities. The refined cell parameters are $a = 5.504$ Å, $b = 7.778$ Å, and $c = 5.528$ Å ($\alpha = \beta = \gamma = 90°$ and $a \neq b \neq c$), therefore the cell volume is 236.723 Å^3. The tolerance factor is used to predict the stability of the $Pr_{0.67}Ba_{0.33}MnO_3$, which is $\tau = 0.9241$. Fourier transform infrared spectroscopy (FTIR) reveals that the Mn-O bonds appear at 600 cm^{-1}. In addition, morphology SEM revealed that the grain sizes are heterogeneous, and the grain shapes are irregular. Using EDX technique, the percentage elemental composition of Pr, Ba, Mn, and O was determined. The values of the atomic percentages for each element are almost identical to the ratios of the elements during sample preparation.

1. Introduction

Mixed-valent perovskite manganites with the general formula R1-xAxMnO3 (R = rare earth elements; A = Ca, Sr, Ba, etc.) have been extensively studied due to the very interesting phenomenon of colossal magnetoresistance (CMR)[1,2] . CMR has gained attention given the potential application of perovskite manganite in magnetic information storage, spintronic application, magnetic refrigeration, and magnetic field sensor. Therefore, researchers start to explore the mechanism of the structural, morphology, transport, and magnetic characteristics to understand the physical properties of perovskite manganite [3]. The perovskite structure generally shows a transformation as the presence of lattice distortion due to modification of the concentration of chemical components in the sample. Differences in the atomic radii of elements at A or Mn site can lead to a complicated behaviour of the sample due to changes in ordering in perovskite layers [4].

---

* *Corresponding author.*
E-mail address: zakiah626@uitm.edu.my

Doping is an effective method used to alter the structure of manganites to obtain their desirable properties. According to previous research, Pr-based manganites are an essential member of the manganite family. Doping amount plays a crucial role in structural, transport and magnetic-phase modifications. As Pr in the A site is partially replaced by Ba in Pr0.67Ba0.33MnO3, the sample undergoes two types of metal-insulator (MI) phase transition [5]. In general, the double-exchange transition between Mn3+ and Mn4+ forms a ferromagnetic metallic state; however, the competition between double-exchange and super-exchange competition mechanism as well as the grain size effect possibly due to distortion in Pr0.67Ba0.33MnO3 leads to Tp1 = 194 K and Tp2 = 160 K [6]. By contrast, the X-ray diffraction patterns of La0.67Ca0.33Mn0.7B0.3O3 revealed the presence of two crystalline phases of manganites, resulting in two broad MI [7]. A recent work reported the electrical and magnetic properties of Pr0.67Ba0.33MnO3, but information on crucial structural and morphological parameters remains inadequate.

The structure and morphology of Pr0.67Ba0.33MnO3 have been investigate in this study. Sample of Pr0.67Ba0.33MnO3 was prepared using solid-state reaction method, and their structural were analysed with XRD and FTIR. In addition, SEM is utilized to investigate the element's composition in minute detail.

2. Methodology

The conventional solid-state method was employed for the preparation of sample $Pr_{0.67}Ba_{0.33}MnO_3$. The following chemical reaction was utilized for measuring the proper stoichiometry ration of the powder compound Pr_6O_{11} (99.99%), BaO_2 (99.99%), and MnO_2 (99.99%).

These powders were weighed and ground for approximately two hours in a dry environmental using agate mortar and pestle to achieve uniform particles. To decompose the carbonates, the mixtures were calcined at 800 C° at a heating rate of 15 C° min^{-1} and cooled at 1 C° min^{-1} for approximately 24 hours in the air. After that, the powders were ground for an additional hour to obtain fine powders and recalcined at 1000 C° for 24 hours to increase the sample's purity and eliminate any secondary phase. After an hour of final grinding, the obtained powder was pressed into a pellet with diameter of 13 mm and thickness of 3 mm using a 5 ton press and then sintered at 1100 C° for 24 hours.

The structural properties of the sample were measured by XRD analysis using a PANanalytical model Xpert PRO MPD diffractometer [8] with Cu-K_α (λ= 1.5418 nm) radiation in Bragg's angle (2θ) ranging from 15° to 80° at room temperature. Rietveld technique was used to obtain the structural parameter of the sample by refining the XRD data with the general structure analysis system (GSAS) program and graphical user interface (EXPUI). The results were visualised for electronic and structure analysis (VESTA) program. The morphology of the sample was analysed using a LEO Gemini 982 SEM, and its elemental composition was determined using EDX method. Fourier transform infrared spectroscopy (FTIR) [9] results were obtained using FTIR-Raman Drift Nicolet 6700 in the range of 450-1500 cm^{-1} to directly probe the functional group present in the perovskite samples. Prior to characterisation, the samples were thoroughly mixed in KBr.

3. Result
3.1 Crystal Structure

XRD technique is crucial to investigate the crystal structure of the sample. The XRD pattern indicates that $Pr_{0.67}Ba_{0.33}MnO_3$ has a single phase without a detectable secondary phase and impurities. Figure 1 (a) shows that all the diffraction peaks are sharp, clear, and well defined,

indicating the well-crystallised sample and good preparation. To have a better understanding of the collected X-ray data, we conducted Rietveld refinement on GSAS, EXPGUI and VESTA programs. Figure 1 (b) shows the Rietveld refinement result of $Pr_{0.67}Ba_{0.33}MnO_3$. The refined pattern is accepted as the obtained value of the agreement factor; χ^2 shows a low value of $\sim$1, which indicates that the fitting is of good quality [10]. The small difference between the observed and calculated data at the bottom of the X-ray diffraction curve indicates the good quality of refinement [10]. All the detailed structural parameters such as refined cell parameters, detailed atomic position, lattice parameter and volume obtained from the refinement are presented in Table 1. The minimum value of χ^2 = 3.308, R_{wp} (%) = 4.1 and R_p (%) = 5.6 indicate that the fitting is properly matched with the experimental result. Pr was positioned at site 4c(x,0.25,z), Ba was positioned at site 4c(x,0.25,z), Mn was positioned at site 4b(0,0,0.5) and two non-equivalent oxygen atoms were positioned at sites (x,y,z).

Based on the Rietveld refinement, $Pr_{0.67}Ba_{0.33}MnO_3$ is indexed for the orthorhombic perovskite-type structure ($\alpha = \beta = \gamma = 90°$ and $a \neq b \neq c$) with a *Pnma* space group. The lattice parameters are a = 5.504 Å, b = 7.778 Å, and c = 5.528 Å, therefore the cell volume is 236.723 Å^3. It is clear that the unit cell volume change due to substitution of Ba (1.47 Å) at Pr (1.179 Å) which is consistent with the previous report [6].
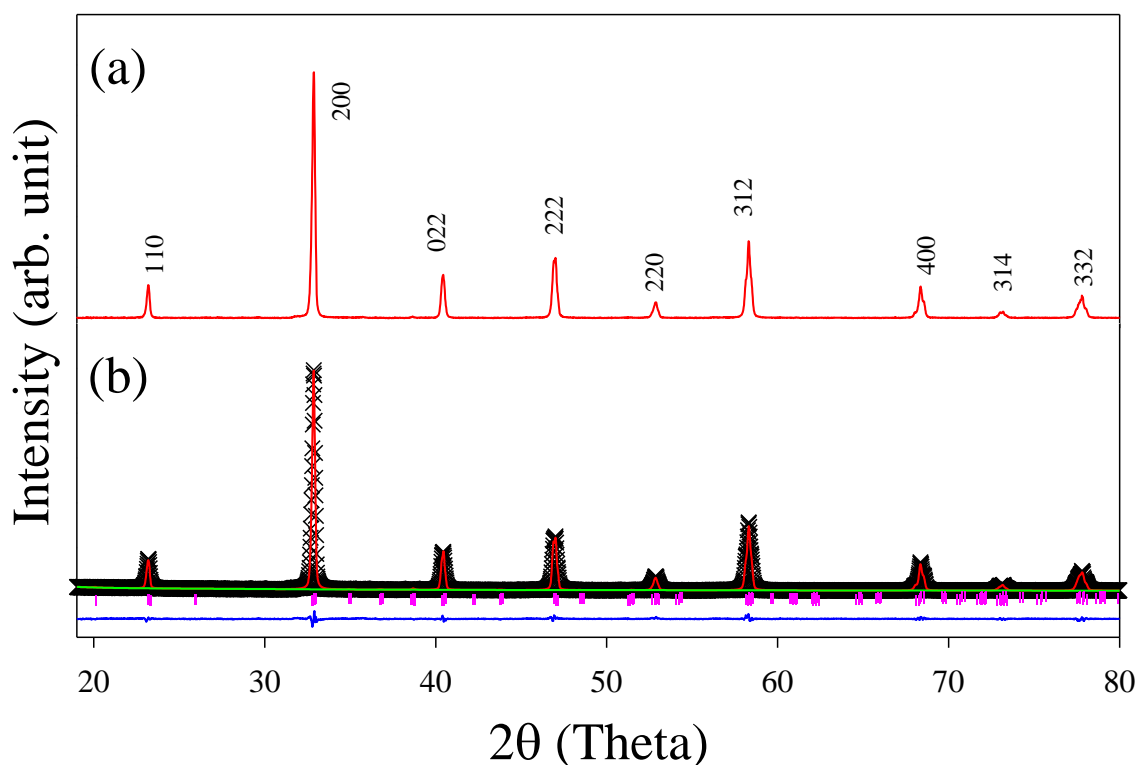
Fig. 1. (a) X-ray diffraction and (b) Rietveld refinement of X-tray diffraction for $Pr_{0.67}Ba_{0.33}MnO_3$ at room temperature. Key: observed (cross), calculated (continuous line) and difference (continuous bottom line), and vertical tick marks above the difference plot show the Bragg peak positions

Table 1
Lattice parameters, unit cell volume, and
goodness of fit for $Pr_{0.67}Ba_{0.33}MnO_3$

Parameter	$Pr_{0.67}Ba_{0.33}MnO_3$
Symmetry	Orthorhombic
Space Group	*Pnma*
a (Å)	5.504
b (Å)	7.778
c (Å)	5.528
V (Å)	236.723
$\alpha = \beta = \gamma$	90
χ^2	3.308
Mn-O_1 (Å)	1.945
Mn-O_2 (Å)	1.951
<Mn-O>(Å)	1.948
Mn-O_1-Mn (∘)	177.113
Mn-O_2-Mn (∘)	176.429
<Mn-O-Mn> (∘)	176.271
R_P (%)	5.6
R_{WP} (%)	4.1
$<r_A>$	1.108
$<r_B>$	0.607
τ	0.928
D (nm)	38×10^{-9}

According to the previous study, we assume that $Pr_{0.67}Ba_{0.33}MnO_3$ is distorted due to the different sizes of atoms and the pores which they occupy as well as due to the Jahn–Teller effect, leading to less symmetric orthorhombic crystal structure [11]. These distortions are principally given by the relationship between the ionic radius of the cations, defined by the tolerance factor [12,13]:

$$\tau = \frac{<r_A> + r_O}{\sqrt{2} \, (<r_B> + r_O)} \tag{1}$$

where '*r*' is the radius of the ion, r_A is the average ionic radii of the A-site, r_B is the average ionic radii of B-site and r_O is the ionic radii of oxygen anion, which are found in the table of Shannon [14]. Based on the calculation, the distortion in $Pr_{0.67}Ba_{0.33}MnO_3$ is τ = 0.928. This result satisfied the requirement for a stable perovskite structure, which is often seen in the range of 0.928 to 1.02, indicating the presence of little distortion [13]. Based on Figure 2, the structure of $Pr_{0.67}Ba_{0.33}MnO_3$ was displayed into four colours where Pr/Ba cations are yellow/green, which was surrounded by 12 oxygens, purple represents Mn and red represents O. The octahedral MnO_6 formed by the position of Mn ions at the B-site which was surrounded by six oxygens ions. The bond lengths and bond angle between Mn and O were 1.945 Å and 176.271°. It is believed that the distortion in the sample influences the results of bond length and bond angle of Mn and O [15]. Therefore, to gain insight into the distortion, one electron bandwidth, *w* of $Pr_{0.67}Ba_{0.33}MnO_3$ electrons, which depends on the Mn-O-Mn bond angle and Mn-O length was calculated using the equation presented below [16,17]:

$$w = \cos \frac{1}{2} (\pi - \gamma) / (d_{Mn-O})^{3.5} \tag{2}$$

where γ is the average Mn-O-Mn bond angle, and d is the average Mn-O bond length. By using the data obtained from the refinement, the calculated value of *w* is 6.308×10^{-3} (Table 1). Crystallite size

D was calculated using the Scherrer equation for the full width at half maximum and integral breadth of reflection (110). In the Scherrer equation below [18,19]:

$$D = \frac{K\lambda}{\beta\,(\theta)\,\cos\theta} \qquad (3)$$

where D is the crystallite size (nm); K is a constant with 0.94; λ is the wavelength of XRD, which is 0.1541 nm for CuK_α radiation Å; β is the full width at half maximum (FWHM) in radians and after subtracting the observed data and reference, in radians; and θ is the angle of the most intense peak of XRD in radians. Therefore, average crystallite size values were found in the range of 38 nm.
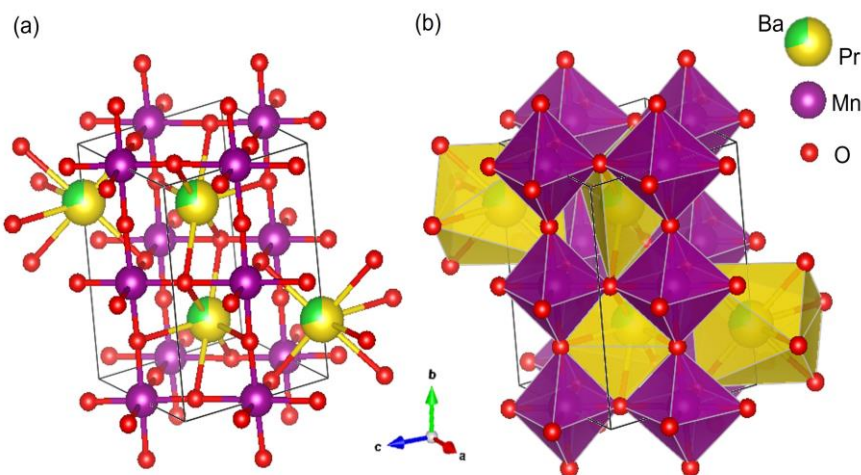
Fig. 2. Structure of $Pr_{0.67}Ba_{0.33}MnO_3$, where the Pr and Ba 12-fold coordinated, and Mn is 6-fold coordinated with the (a) crystallographic and (b) polyhedral

Figure 3 shows the FTIR spectra within the wavenumber range of 450–1600 cm^{-1}. The result shows a broad peak at a wavenumber of 600 cm^{-1} [20]. Therefore, the sample contained metal-oxygen bonds corresponding to the Mn-O-Mn bond length, as confirmed by the internal motion causing the stretching mode. The results obtained is in line with the findings of Xia *et al.,* [21], that in reported in $Ln_{0.67}Ca_{0.33}MnO_3$ (Ln = La, Pr, Nd and Sm) manganites
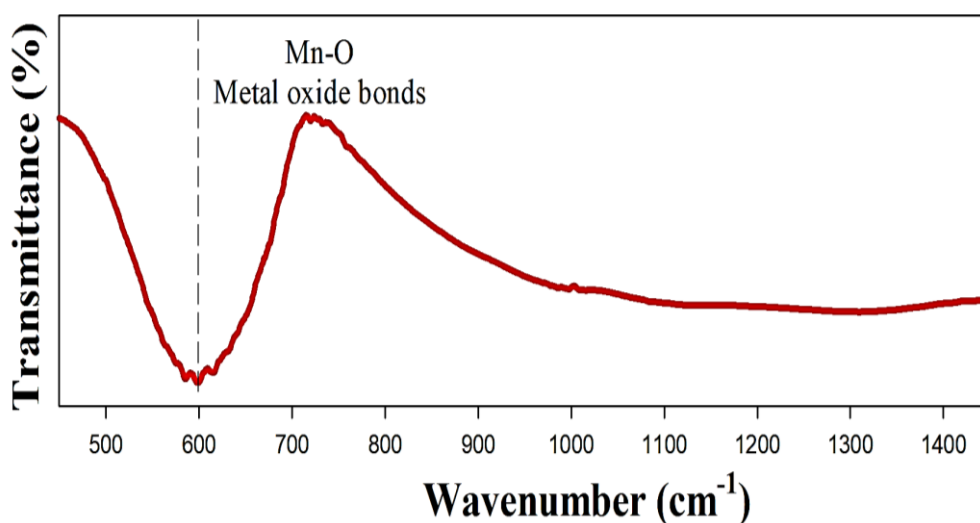
Fig. 3. Fourier transform infrared (FTIR) spectra of $Pr_{0.67}Ba_{0.33}MnO_3$

3.2 Morphology (Microstructural Analysis)

The surface morphology of $Pr_{0.67}Ba_{0.33}MnO_3$ was determined by SEM (Figure 4). The sample contains nonhomogeneous grains with irregular shape. Similar finding is reported that the irregular grains contribute to lattice strain, which randomly displaces oxygen ions [22]. This distortion of MnO6 octahedra leads to the localisation of electrons. In fact, a significant defect in the A-site cations results in a random arrangement of the Mn^{3+} and Mn^{4+} ions [22,23]. According to the morphology, the average diameter of $Pr_{0.67}Ba_{0.33}MnO_3$ is 2.312 μm by using the scale of 20 μm in Figure 4. The observed result is consistent with $Pr_{0.67}Ba_{0.33}MnO_3$ [5] and $Pr_{1-x}Ba_xMnO_3$ $(0.25 \leq x \leq 0.36)$ [24]. According to the quantitative element analysis by using EDX, the sample only contains praseodymium (Pr), barium (Ba), manganese (Mn) and oxygen (O). The atomic percentage of the sample in the inset of Figure 5 shows the presence of all elements in the sample as well as close to the nominal ones (Pr: Ba: Mn: O = 13.4: 6.6: 20: 60). Therefore, the EDAX result of $Pr_{0.67}Ba_{0.33}MnO_3$ supports the stoichiometric compositions.

Fig. 4. SEM micrograph sample
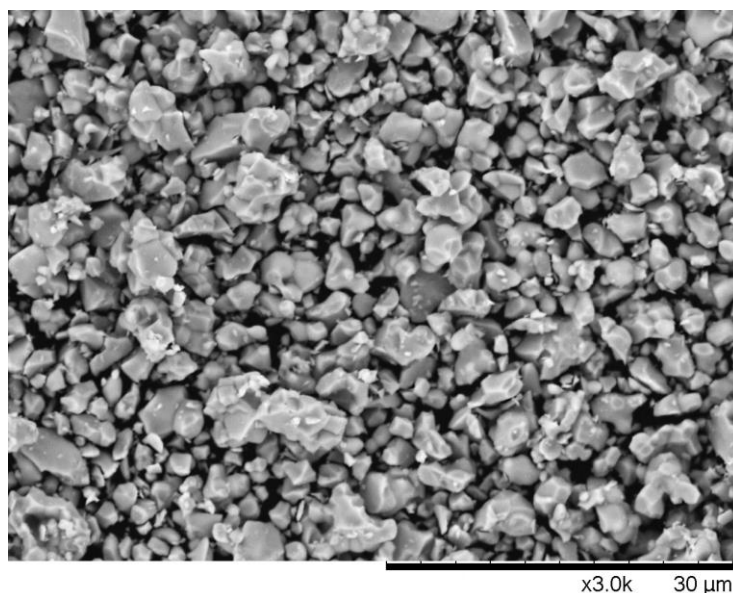

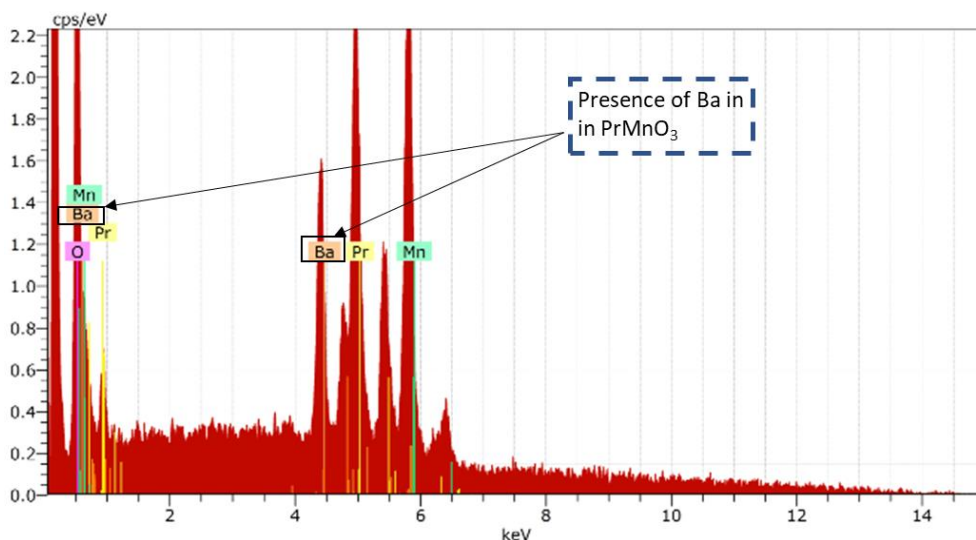**Fig. 5.** EDX of $Pr_{0.67}Ba_{0.33}MnO_3$ sample

4. Conclusions

In summary, we synthesised crystallised PBMO through solid-state reaction and studied its detailed structure. The sample is a single-phased crystal with an orthorhombic structure and *Pnma* space group. It has a unit cell volume of 236.723 Å^3 and non-homogenous morphology. The morphology is slightly changed because of the Ba atom being added to the Mn site, which is crucial to reconfirm the effect of Ba doping on the structure. The calculated tolerance factor, one electron bandwidth and Scherrer equation were 0.928, 6.308×10^{-3} and 38×10^{-9}, respectively. The FTIR spectrum shows the significant absorption bands at $600\ \text{cm}^{-1}$, indicating the formation of Mn bond and manganite.

References

[1] Tokura, Yoshinori, and Yasuhide Tomioka. "Colossal magnetoresistive manganites." *Journal of Magnetism And Magnetic Materials* 200, no. 1-3 (1999): 1-23. https://doi:10.1016/S0304-8853(99)00352-2

[2] Dagotto, Elbio, Takashi Hotta, and Adriana Moreo. "Colossal magnetoresistant materials: the key role of phase separation." *Physics reports* 344, no. 1-3 (2001): 1-153. https://doi.org/10.1016/S0370-1573(00)00121-6

[3] Venkateshwarlu, D., Himanshu Dadhich, Bhargav Rajyaguru, Sukriti Hans, M. Ranjan, R. Venkatesh, V. Ganesan, P. S. Solanki, and N. A. Shah. "Semiconducting nature and magnetoresistance behaviour of ZnO/La0. 3Ca0. 7MnO3/SrTiO3 heterostructures." *Materials Science in Semiconductor Processing* 136 (2021): 106154. https://doi:10.1016/j.mssp.2021.106154

[4] Hsini, M., L. Ghivelder, and F. Parisi. "Critical behavior investigated through magnetocaloric effect in PrSrMnO and Pr (Sr, Ca) MnO manganites." *Journal of Magnetism and Magnetic Materials* 535 (2021): 168059. https://doi:10.1016/j.jmmm.2021.168059

[5] Panwar, Neeraj, S. K. Agarwal, G. L. Bhalla, Davinder Kaur, and D. K. Pandya. "Structural, Electrical And Magnetic Properties of Pr 1-x Ba x MnO 3 (x= 0.33–0.80)." *International Journal of Modern Physics B* 21, no. 15 (2007): 2647-2656. https://doi.org/10.1142/S0217979207037284

[6] Hcini, S., S. Zemni, A. Triki, H. Rahmouni, and Michel Boudard. "Size mismatch, grain boundary and bandwidth effects on structural, magnetic and electrical properties of Pr0. 67Ba0. 33MnO3 and Pr0. 67Sr0. 33MnO3 perovskites." *Journal of Alloys and Compounds* 509, no. 5 (2011): 1394-1400. https://doi:10.1016/j.jallcom.2010.10.190

[7] Kolat, V. S., H. Ü. S. E. Y. İ. N. Gencer, M. Gunes, and S. E. L. Ç. U. K. Atalay. "Effect of B-doping on the structural, magnetotransport and magnetocaloric properties of La0. 67Ca0. 33MnO3 compounds." *Materials Science and Engineering: B* 140, no. 3 (2007): 212-217. http://doi:10.1016/j.mseb.2007.05.002

[8] Hamzah, Sofiah, Mohd Sabri Mohd Ghazali, Norhafiza Ilyana Yatim, Jamali Sukaimi, and Maslinda Alias. "Characterization Studies of Integrated Hydroxyapatite FROM Fish Scale and Polyether Sulfone Membrane for Ion Excahnge Membrane Preparation." *Journal of Advanced Research in Applied Sciences and Engineering Technology* 17, no. 1 (2019): 1-12.

[9] Abd Razak, Noor Harliza, Siti Nadzirah Mohd Nawi, and Ku Halim Ku Hamid. "Characterization Of Chitin With Extraction Leucaena Leucephala Pods Using Hydrochloric Acid (HCl) By Fourier Transform Infrared." *Journal of Advanced Research in Applied Sciences and Engineering Technology* 17, no. 1 (2019): 21-28.

[10] Toby, Brian H. "R factors in Rietveld analysis: How good is good enough?." *Powder diffraction* 21, no. 1 (2006): 67-70. https://doi.org/10.1154/1.2179804

[11] Kugel, Kliment I., and D. I. Khomskiĭ. "The Jahn-Teller effect and magnetism: transition metal compounds." *Soviet Physics Uspekhi* 25, no. 4 (1982): 231. https://doi.org/10.1070/PU1982v025n04ABEH004537

[12] Ibrahim, N., A. K. Yahya, S. S. Rajput, S. Keshri, and M. K. Talari. "Double metal–insulator peaks and effect of Sm3+ substitution on magnetic and transport properties of hole-doped La0. 85Ag0. 15MnO3." *Journal of magnetism and*

magnetic materials 323, no. 16 (2011): 2179-2185. http://doi:10.1016/j.jmmm.2011.03.027

[13] Asmira, Nor, N. Ibrahim, Z. Mohamed, and A. K. Yahya. "Effect of Cr3+ substitution at Mn-site on electrical and magnetic properties of charge ordered Bi0. 3Pr0. 3Ca0. 4MnO3 manganites." *Physica B: Condensed Matter* 544 (2018): 34-46. https://doi.org/10.1016/j.physb.2018.05.020

[14] Shannon, RD T., and C. T. Prewitt. "Revised values of effective ionic radii." *Acta Crystallographica Section B: Structural Crystallography and Crystal Chemistry* 26, no. 7 (1970): 1046-1048. http://doi:10.1107/S0567740870003576

[15] Geddo Lehmann, Alessandra, Giuseppe Muscas, Maurizio Ferretti, Emanuela Pusceddu, Davide Peddis, and Francesco Congiu. "Structural and Magnetic Properties of Nanosized Half-Doped Rare-Earth Ho0. 5Ca0. 5MnO3 Manganite." *Applied Sciences* 12, no. 2 (2022): 695. https://doi.org/10.3390/app12020695

[16] Rozilah, R., M. K. Yaakob, and A. K. Yahya. "Effect of Ni substitution at Mn-site on structural and electronic properties of monovalent-dopedPr0. 75Na0. 25MnO3 manganite: Experimental and first principles LDA+ U studies." *Physica B: Condensed Matter* 579 (2020): 411904. https://doi.org/10.1016/j.physb.2019.411904

[17] Xu, Sheng, Yutaka Moritomo, Kenji Ohoyama, and Arao Nakamura. "Neutron Structural analysis of La1-x Sr x MnO3– Variation of One-Electron Bandwidth W with Hole Doping–." *Journal of the Physical Society of Japan* 72, no. 3 (2003): 709-712. https://doi.org/10.1143/JPSJ.72.709

[18] Aziz, S. S. S. A., N. Ibrahim, R. Rajmi, and Z. Mohamed. "Magnetic properties and evolution of magnetoresistance effect in Pr0. 75Na0. 05K0. 20Mn1–x Fe x O3 with 0≤ x≤ 0.04." *Applied Physics A* 128, no. 10 (2022): 940. https://doi.org/10.1143/JPSJ.72.709

[19] Monshi, Ahmad, Mohammad Reza Foroughi, and Mohammad Reza Monshi. "Modified Scherrer equation to estimate more accurately nano-crystallite size using XRD." *World journal of nano science and engineering* 2, no. 3 (2012): 154-160. https://10.4236/wjnse.2012.23020

[20] Mohamed, Zakiah, Intan Syazwani Shahron, Norazila Ibrahim, and Mohd Fauzi Maulud. "Influence of ruthenium doping on the crystal structure and magnetic properties of Pr0. 67Ba0. 33Mn1–xRuxO3 manganites." *Crystals* 10, no. 4 (2020): 295. https://doi.org/10.3390/cryst10040295

[21] Xia, Weiren, Kai Leng, Qingkai Tang, Li Yang, Yuting Xie, Zhiwei Wu, and Xinhua Zhu. "Comparative studies on the structural, magnetic, and optical properties of perovskite Ln0. 67Ca0. 33MnO3 (Ln= La, Pr, Nd, and Sm) manganite nanoparticles synthesized by sol–gel method." *AIP Advances* 11, no. 3 (2021): 035007. https://doi.org/10.1063/5.0036723

[22] Koc, N. Soylu, S. P. Altintas, N. Mahamdioua, and C. Terzioglu. "Cation size mismatch effect in (La1-yREy) 1.4 Ca1. 6Mn2O7 perovskite manganites." *Journal of Alloys and Compounds* 797 (2019): 471-476. https://doi.org/10.1016/j.jallcom.2019.05.079

[23] Lim, K. P., S. W. Ng, L. N. Lau, MM Awang Kechik, S. K. Chen, and S. A. Halim. "Unusual electrical behaviour in sol–gel-synthesised PKMO nano-sized manganite." *Applied Physics A* 125 (2019): 1-10. https://doi.org/10.1007/s00339-019-3046-2

[24] Xin, Yang, Lei Shi, Jiyin Zhao, Xueyou Yuan, Li Hou, and Ruixue Tong. "Electrical transport properties driven by magnetic competition in hole-doped perovskite Pr1-xBaxMnO3 (0.25≤ x≤ 0.36)." *Ceramics International* 47, no. 14 (2021): 19464-19470. https://doi.org/10.1016/j.ceramint.2021.03.283